HHS Public Access

Author manuscript

Sci Signal. Author manuscript; available in PMC 2016 January 21.

Published in final edited form as:

Sci Signal. ; 8(386): ra73. doi:10.1126/scisignal.aaa4374.

Reversal of diet-induced obesity and insulin resistance by inducible genetic ablation of GRK2

Rocio Vila-Bedmar[1,2], **Marta Cruces-Sande**[1,2,#], **Elisa Lucas**[1,2,#], **Hanneke L.D.M. Willemen**[3], **Cobi J. Heijnen**[3,4], **Annemieke Kavelaars**[3,4], **Federico Mayor Jr.**[1,2,*], and **Cristina Murga**[1,2,*]

[1]Centro de Biología Molecular Severo Ochoa (CSIC-UAM), Madrid, Spain [2]Instituto de Investigación Sanitaria La Princesa, Madrid, Spain [3]Laboratory of Neuroimmunology and Developmental Origins of Disease (NIDOD), University Medical Center Utrecht, Utrecht 3584 EA, The Netherlands [4]Laboratory of Neuroimmunology, Department of Symptom Research, Division of Internal Medicine, The University of Texas M.D. Anderson Cancer Center, Houston, TX

Abstract

Insulin resistance is a common feature of obesity and predisposes individuals to various prevalent pathological conditions. G protein-coupled receptor kinase 2 (GRK2) integrates several signal transduction pathways and is emerging as a physiologically relevant inhibitor of insulin signaling. GRK2 abundanceis increased in humans with metabolic syndrome and in different murine models of insulin resistance. To support GRK2 as a potential drug target in type 2 diabetes and obesity, we investigated whether lowering GRK2 abundance reversed an ongoing systemic insulin-resistant phenotype, using a mouse model of tamoxifen-induced GRK2 ablation after high fat diet-dependent obesity and insulin resistance. Tamoxifen-triggered GRK2 deletion impeded further body weight gain, normalized fa sting glycemia, improved glucose tolerance and was associated with preserved insulin sensitivity in skeletal muscle and liver, thereby maintaining whole body glucose homeostasis. Moreover, when continued to be fed a high fat diet, these animals displayed reduced fat mass and smaller adipocytes, were resistant to the development of liver steatosis, and showed reduced expression of pro-inflammatory markers in the liver. Our results indicate that GRK2 acts as a hub to control metabolic functions in different tissues, which is key to controlling insulin resistance development in vivo. These data suggest that inhibiting GRK2 could reverse an established insulin-resistant and obese phenotype, thereby putting forward this enzyme as a potential therapeutic target linking glucose homeostasis and regulation of adiposity.

[*]Corresponding authors. Contact information: Centro de Biologia Molecular “Severo Ochoa”, C/Nicolás Cabrera 1, Universidad Autónoma de Madrid, 28049 Madrid, Spain., cmurga@cbm.csic.es; Phone 34-91-1964641; Fax: 34-91-196-4420, fmayor@cbm.csic.es; Phone: 34-91-1964626; Fax: 34-91-196-4420.
[#]These authors contributed equally to this work

Author Contributions: RVB, designed and performed experiments, prepared figures, analyzed data, wrote and revised manuscript. EL and MCS, performed experiments, prepared figures and revised manuscript. HW, performed experiments. CH and AK, analyzed data and revised manuscript. FM Jr, and CM designed experiments, analyzed data, wrote and revised manuscript.

Competing Interests: The authors declare that they have no competing interests.

INTRODUCTION

Insulin resistance is characterized by a reduced responsiveness to circulating insulin, and is a common feature of obesity that predisposes to several pathological conditions, including hyperinsulinemia, glucose intolerance, hypertension, non-alcoholic fatty liver disease (NAFLD), cardiovascular disease, and type 2 diabetes, and is becoming a global public health problem (1). A better knowledge of how different intracellular pathways integrate to fine-tune the response to insulin, body weight gain and metabolic rate might help identify novel therapeutic strategies beyond diet control, physical exercise and currently used pharmaceutical agents.

G protein-coupled receptor kinase 2 (GRK2) has been widely studied for its role in the desensitization of G protein-coupled receptors (GPCRs) (2). GRK2 can also impact cell signaling networks by directly interacting with and/or phosphorylating non-GPCR components of transduction cascades, and thus has emerged as an integrative node of cellular networks (3–5). Since Anis et al. (6) have demonstrated that peptide GRK2 inhibitors ameliorate glucose homeostasis in different animal models of diabetes, several reports have put forward a role for GRK2 in the regulation of insulin response (7, 8). GRK2 abundance is increased in blood mononuclear cells from metabolic-syndrome patients and in different models of insulin resistance, such as human visceral adipocytes, and in white adipose tissue (WAT) and muscle of TNFα-, aging- or high-fat diet (HFD)-induced murine models, suggesting that increased GRK2 abundance may contribute to the development or maintenance of this condition. Moreover, enhanced GRK2 abundance decreases insulin sensitivity in several cell types and tissues (9). On the other hand, GRK2 inhibits β-adrenergic receptors (βAR) and decreased GRK2 abundance enhances energy expenditure and thermogenesis in brown adipose tissue (BAT), at least partially by increasing adrenergic signaling (10). Cardiac GRK2 may also participate in the cross-talk between adrenergic and insulin receptor pathways (11, 12).

Overall, these data suggest that GRK2 may act as a global metabolic regulator due to its ability to directly target both the insulin cascade and key GPCRs related to insulin sensitivity and metabolism. To support GRK2 as a potential drug target in type 2 diabetes and obesity, it would be necessary to show that loss of GRK2 can revert an ongoing systemic insulin resistance phenotype. Apart from certain peptides and serotonin reuptake inhibitors that also have an effect on GRK2 (6, 13, 14), specific GRK2 inhibition must be achieved by indirect genetic means. Thus, we used a tamoxifen (Tam)-inducible GRK2 deletion mouse model, which allowed us to ablate GRK2 after HFD-induced obesity and insulin resistance developed, which would mimic some aspects of the effects of a putative GRK2 inhibitory drug. We show that decreasing GRK2 abundance reversed key systemic and tissue-specific aspects of an established insulin-resistant and obese phenotype, thus revealing that targeting GRK2 may allow for the multi-tissue treatment of metabolic disorders related to obesity.

RESULTS

Tamoxifen-induced GRK2 deletion during a HFD prevents further body weight gain and restores glucose tolerance and global insulin sensitivity

$Cre^{-/-}GRK2^{fl/fl}$ animals (Tam-$GRK2^{+/+}$), used as controls, and $Cre^{+/-}GRK2^{fl/fl}$ mice, that undergo GRK2 deletion upon tamoxifen treatment (Tam-$GRK2^{-/-}$ animals), were fed either a standard diet (SD) or transferred to a HFD for 8 weeks (Suppl. Fig. 1A). At this point we evaluated the increase in body weight, fasting glucose concentrations and the onset of systemic insulin resistance in the animals fed a HFD compared with their SD-fed littermates (Suppl. Fig. 1B–D). Once diet-induced insulin resistance and obesity were confirmed in both genotypes, mice were injected with tamoxifen and maintained for 5 more weeks on a HFD. Tamoxifen injection markedly decreased GRK2 protein abundance in several tissues in Tam-$GRK2^{-/-}$ mice (Suppl. Fig. 1E). The extent of GRK2 loss ranged from 60 to 80% depending on the organ, consistent with the reported variability in the extent of Cre-mediated recombination in different tissues (15) and with published work (16). Body weight did not differ between the two groups during the 8 weeks of HFD prior to tamoxifen injection (Figure 1A). As reported (17), the administration of tamoxifen for 5 days caused a transient decrease in body weight in both groups of mice. However, control mice (Tam-$GRK2^{+/+}$) continued to gain weight after tamoxifen injection throughout the five additional weeks of HFD, whereas further body weight gain was prevented in Tam-$GRK2^{-/-}$ mice (Figure 1A and Suppl. Fig. 2) relative to both control Tam-$GRK2^{+/+}$ animals and also to $Cre^{+/-}$ mice without floxed GRK2 alleles (Tam-$Cre^{+/-}$) (Suppl. Fig. 3A). We cannot rule out that control and Tam-$GRK2^{-/-}$ animals present a differential sensitivity to tamoxifen treatment, which might influence subsequent body weight gain. However, the initial decrease in body weight upon tamoxifen injection was similar in both mouse genotypes (Figure 1A), suggesting that tamoxifen treatment per se does not have a major impact on the differences in body weight observed along the following weeks. Food intake did not differ between genotypes (Figure 1B).

Tam-$GRK2^{+/+}$ mice showed a significant deterioration in glucose tolerance at the end of the experimental protocol (13 weeks of HFD), indicating a progressive intensification of insulin resistance during the 5 additional weeks of HFD feeding. In contrast, Tam-$GRK2^{-/-}$ mice showed improved glucose homeostasis (Figure 1C–D) suggesting that the previously observed glucose intolerance was reversed. Accordingly, the area under the curve showed a significant enhancement of glucose tolerance in Tam-$GRK2^{-/-}$ mice at the end of the HFD feeding period (Figure 1E).

Consistent with the glucose tolerance tests, control Tam-$GRK2^{+/+}$ mice displayed decreased insulin sensitivity throughout the progression of the HFD (Figure 1F), whereas Tam-$GRK2^{-/-}$ mice showed significantly enhanced insulin sensitivity at the end of the HFD after Tam-induced GRK2 deletion compared to before tamoxifen administration or to control littermates (Figure 1G–H), indicating that the improved glucose homeostasis in Tam-$GRK2^{-/-}$ mice could be attributed to enhanced global insulin sensitivity. In addition, GRK2 deletion after 8 weeks of HFD reduced fasting glucose plasma concentrations in the face of high fat feeding, without increasing insulinemia (Figure 1I–J), indicating that Tam-$GRK2^{-/-}$

mice were protected against the hyperglycemia and hyperinsulinemia characteristic of insulin-resistant and pre-diabetic states. These results demonstrated that GRK2 depletion during diet-induced obesity and insulin resistance resulted in improved whole-body glucose homeostasis and enhanced insulin sensitivity.

GRK2 depletion enhances insulin-induced phosphorylation of AKT in peripheral tissues

Skeletal muscle is the major site for insulin-induced glucose disposal and a decreased insulin response in this tissue is the initiating defect in insulin-resistant states during the development of type 2 diabetes (18). Consistent with the increased glucose tolerance and enhanced insulin sensitivity in Tam-GRK2$^{-/-}$ mice, GRK2 ablation restored insulin-induced phosphorylation of AKT at Ser^{473} in muscle (Figure 2A). Moreover, insulin-induced AKT phosphorylation was also enhanced in Tam-GRK2$^{-/-}$ mice in other tissues that are key for metabolic regulation, such as epididymal WAT (eWAT) and liver (Figures 2B–C), although the increase was not statistically significant in eWAT. Insulin-induced phosphorylation of AKT was similar in post-tamoxifen Cre$^{+/-}$ mice (Tam-Cre$^{+/-}$) and Cre$^{-/-}$ animals (Tam-Cre$^{-/-}$, used as controls) (Suppl. Fig. 3B), thus discarding non-specific effects due to Tam-induced Cre nuclear translocation in the analyzed tissues. Control Tam-GRK2$^{+/+}$ and Tam-GRK2$^{-/-}$ mice did not differ in the abundance of inhibitors of insulin signaling (PTP1B and PTEN) or of key insulin transduction partners (p110β, p85β, IRS1 or IRS2) (Suppl. Fig. 4) that could explain the insulin-sensitizing effect of low GRK2 abundance. Overall, these data indicate that GRK2 depletion in Tam-treated mice plays a relevant role in the preservation of insulin sensitivity in the analyzed tissues, probably through already described mechanisms (9), and that this insulin sensitization can explain the improved glucose homeostasis caused by reducing GRK2 abundance during a HFD.

Inducible loss of GRK2 is associated with reduced epididymal fat pad weight

Epididymal fat pad weight was reduced in HFD-fed Tam-GRK2$^{-/-}$ mice compared to HFD-fed control mice (Figure 3A). Histological analysis revealed a significantly greater frequency of small adipocytes and a lower frequency of mid-sized and large adipocytes in eWAT from these mice (Figure 3B). Tam-GRK2$^{-/-}$ mice displayed no differences in the abundance of C/EBPα, a transcription factor that promotes preadipocyte differentiation, or PPARγ, another transcription factor that is key for adipogenesis (19) (Figure 3C), suggesting that impaired differentiation did not cause the decrease in adipocyte size. Moreover, the increase in both protein abundance and gene expression of hormone-sensitive lipase (HSL), a critical enzyme for cAMP-dependent lipolysis (20) (Figure 3D) in Tam-GRK2$^{-/-}$ mice suggested that the decrease in fat mass was due to enhanced lipolysis in eWAT. Indeed, the eWAT depot from Tam-GRK2$^{-/-}$ mice showed an enhanced ex vivo response to the β-adrenergic agonist isoproterenol (Figure 3E) and HFD-fed Tam-GRK2$^{-/-}$ mice had a 30% increase in circulating free fatty acids (FFAs) in the fasted but not in the fed state (Figure 3F). These results indicate a blunted lipolytic response to fasting in HFD-fed control mice that was absent in Tam-GRK2$^{-/-}$ mice.

GRK2 ablation increases the expression of thermogenic and fatty acid oxidation markers in brown adipose tissue

By contributing to whole-body fatty acid oxidation and energy expenditure, BAT regulates fat content (21, 22). The BAT of HFD-fed Tam-GRK2$^{-/-}$ mice showed an increased number of smaller adipocytes, which was associated with a higher proportion of multilocular lipid droplets (Figure 4A) suggesting that GRK2 ablation might increase BAT function. The BAT from Tam-GRK2$^{-/-}$ animals showed an increase both in protein and mRNA abundance of carnitine palmitoyltransferase 1 (CPT1), the rate-limiting enzyme that controls fatty acid entry and oxidation in the mitochondria (23) (Figure 4B–C), as well as augmented protein abundance of uncoupling protein 1 (UCP1), which is involved in thermogenesis [reviewed in (22, 24)]. These effects could underlie an increased capacity for fatty acid metabolism and thermogenesis in the BAT of these mice. However, the expression of the mRNAs encoding UCP1 or of its transcriptional activators PPARγ coactivator 1α (PGC1α) (22, 25) or type 2 deiodinase (Dio2) (25), which locally produces T_3 required for the adrenergic induction of UCP1 (26), suggest a post-transcriptional mechanism controlling UCP1 abundance in these mice (Fig. 4C). In brown adipocytes, lipolysis is essential to activate thermogenesis, because it allows the release of fatty acids, which activate UCP1 (24, 27). In line with our observations in WAT, mRNA abundance of the HSL gene (*lipe*) was significantly increased in BAT upon GRK2 deletion (Figure 4C), as was the *ex vivo* lipolytic response of BAT explants from these mice to the β-adrenergic agonist isoproterenol (Figure 4D). These data point to an increased capacity for fatty acid metabolism in Tam-GRK2$^{-/-}$ mice and might explain the absence of lipotoxicity observed in these animals despite the increased plasma free fatty acid availability.

The increased response of adipose tissues after GRK2 deletion to adrenergic input, a key pathway by which the sympathetic nervous system (SNS) modulates energy homeostasis (24, 25, 27), raised the issue of whether this effect was also responsible for the overall glucose homeostasis phenotype of Tam-GRK2$^{-/-}$ animals. To answer this question, glucose tolerance tests were performed in control or GRK2-deleted mice treated with the β-adrenergic antagonist propranolol to abrogate adrenergic input. Propranolol resulted in impaired glucose handling in HFD-fed control mice but not in GRK2-depleted mice (Figure 4E). These data suggest that the improvement in glucose tolerance obtained upon GRK2 depletion prevails even under conditions of adrenergic blockade, and demonstrates that GRK2 loss can influence insulin sensitization independently of its effects on the control of adrenergic stimulation.

GRK2 deletion during HFD feeding protects against the development of NAFLD and decreases the expression of pro-inflammatory markers in the liver

Chronic exposure of mice to HFD induces lipid accumulation in this tissue, leading to NAFLD. Histological analysis revealed marked steatosis in livers of HFD-fed control mice. In contrast, the degree of fat accumulation in the liver was substantially alleviated in HFD-fed Tam-GRK2$^{-/-}$ mice compared to control animals (Figure 5A). Liver weight was also significantly lower after 13 weeks of HFD in Tam-GRK2$^{-/-}$ mice compared to controls (Figure 5B). These effects are consistent with the decreased hepatic lipid accumulation, and unrelated to the presence of Cre (Suppl. Fig. 5). The abundance of lipogenic enzyme fatty

acid synthase (FAS) and the transcription factor PPAR is increased in fatty liver (28, 29); however, Tam-GRK2$^{-/-}$ mice did not show differences in the mRNA expression for the fatty acid entry and oxidation marker *Cpt1a* and reduced mRNA and protein abundance for FAS and PPAR (Figure 5C–D), suggesting decreased lipogenesis.

The inflammatory activation of macrophages and Kupffer cells has been implicated in both obesity-induced insulin resistance and fatty liver disease in parallel with the activation of stress- and inflammation-related kinases (30). Immunostaining and mRNA expression for F4/80, a representative macrophage and Kupffer cell marker, were comparable between HFD-fed control and Tam-GRK2$^{-/-}$ mice (Figure 5E–G). However, in HFD-fed control animals, macrophages frequently aggregated to surround hepatocytes with large intracellular lipid droplets (arrows in Figure 5E), which is reminiscent of hepatic-crown like structures observed in adipose tissue from obese animals and humans and considered to be an indicator of the presence of pro-inflammatory macrophages (24) (31). Notably, HFD-fed Tam-GRK2$^{-/-}$ mice showed a scattered macrophage distribution, with lower numbers of hepatic crown-like structures (Suppl. Fig. 6A). Consistently, the expression of mRNAs characteristic of the pro-inflammatory M1 macrophage phenotype, such as those encoding the inducible nitric oxide synthase (iNOS), as well as the phosphorylation of JNK, a kinase that is involved in inflammation (32), was decreased in Tam-GRK2$^{-/-}$ mice (Suppl. Fig. 6B–C). In addition, the ratio of M2 (anti-inflammatory, Mannose Receptor 1 *(mrc1)*-expressing) to M1 macrophages (pro-inflammatory, (inducible nitric oxide synthase *(nos2)*-expressing) was significantly increased in Tam-GRK2$^{-/-}$ mice (Figure 5H), in accordance with a tendency towards a reduced expression of tumor necrosis factor-alpha-encoding mRNA (*tnfa)* in these mice, indicating that lowering GRK2 abundance decreases HFD-induced hepatic steatosis and inflammation.

DISCUSSION

In this work, we provide evidence that global decrease of GRK2 abundance reversed key systemic and tissue features of an already established insulin-resistant and obese phenotype in HFD-fed mice. Tamoxifen-induced GRK2 deletion reduced further body weight gain despite continued HFD feeding, normalized glucose intolerance, led to improved insulin sensitivity, and prevented the development of adiposity and fatty liver. These data, together with the increase in GRK2 abundance in liver, muscle and WAT in murine insulin resistance experimental models (9) suggest that the ability of GRK2 to control metabolic functions in different tissues is key to the development of insulin resistance *in vivo*. We show here that at least four potentially tissue-specific processes appear to be involved in the physiological effects of GRK2 reduction in HFD-fed mice: improved insulin signaling in peripheral tissues, enhanced lipolysis in WAT and BAT, increased expression of mRNAs encoding proteins involved in fatty acid oxidation and thermogenesis in BAT, and reduced steatosis and in ammation in the liver. We postulate that such pleiotropic effects of GRK2 abundance are due to the ability of GRK2 to directly modulate both the insulin receptor cascade and key GPCRs that control adiposity and metabolic rate such as β-adrenergic receptors.

The glucose-lowering effect of decreasing GRK2 abundance appeared to involve preserved peripheral insulin sensitivity, because insulin-targeted tissues key for glucose homeostasis

exhibited augmented insulin-induced AKT phosphorylation. In addition to these tissue-autonomous effects, part of the enhanced insulin sensitivity of Tam-GRK2$^{-/-}$ mice could be related to their reduced adiposity, decreased fat mass accretion and adipocyte size, and increased lipolysis and enhanced response to adrenergic input in mature WAT adipocytes. However, the potential impact of increased lipolytic flux in the global insulin-resistant phenotype is not straightforward, because a high lipolytic rate can be associated with insulin resistance (33). Conversely, impaired lipolytic capacity has been postulated to result in an improved overall metabolic status, because reduced release of free fatty acids from adipose stores would protect peripheral tissues from lipotoxicity (34, 35). However, some animal models of impaired lipolysis display an overall impairment in systemic metabolic function (36). This finding supports the notion that a decreased release of free fatty acids *per se* does not necessarily predict an improvement of systemic insulin sensitivity, because the deficiency in free fatty acid mobilization as a consequence of reduced WAT metabolic flexibility may cause systemic metabolic dysfunction. Accordingly, despite their enhanced lipolytic phenotype, Tam-GRK2$^{-/-}$ mice did not display signs of lipotoxicity, but rather increased insulin sensitivity. We hypothesize that this apparent paradox could be explained by the improved function of BAT observed upon GRK2 loss, as indicated by the preserved morphology of this tissue and its enhanced adrenergic-induced lipolytic capacity, as well as the increased expression of thermogenic (UCP1) and FA oxidation (CPT1) markers. These changes could allow BAT to act as an efficient “metabolic sink” for the extra free fatty acids produced in WAT (Fig. 6) and might explain the lack of lipotoxicity in Tam-GRK2$^{-/-}$ animals despite the increased plasma free fatty acid concentrations. This explanation is consistent with the increased energy expenditure and enhanced BAT fatty acid oxidation and thermogenic capacity previously reported in GRK2$^{+/-}$ mice (10). The finding that GRK2-depleted animals maintained glucose homeostasis upon propranolol treatment indicates that increased β-adrenergic signaling is not fully responsible for the improvement in glucose tolerance, and that GRK2 loss can influence insulin sensitization independently of its effects on the control of adrenergic stimulation. However, increased adrenergic signaling in these mice could account for other aspects of their phenotype, such as the increased lipolytic capacity and the protection against diet-induced weight gain.

The liver is another key organ for metabolic regulation, and we demonstrated here that decreasing GRK2 abundance protected against HFD-induced hepatic insulin resistance and impaired lipid accumulation, an effect that was associated with reduced expression of the genes encoding FAS and PPARγ, which are increased in fatty liver (29, 37). On the other hand, insulin resistance is increased by the accumulation of macrophages that secrete proinflammatory mediators and by macrophage polarization from an alternative anti-inflammatory M2 activation state to a pro-inflammatory M1 activation state (38). In control HFD-fed mice, macrophages displayed an M1-like pro-inflammatory profile, and were predominantly found surrounding hepatocytes with large lipid droplets in hepatic crown-like structures, which are involved in disease progression from simple steatosis to non-alcoholic steatohepatitis (39). In contrast, livers from HFD-fed Tam-GRK2$^{-/-}$ mice had lower activation of inflammatory pathways such as JNK, a scattered distribution of macrophages, and an increased M2 to M1 ratio. Hepatic macrophages display remarkable plasticity in their activation programs (38) ranging from the activation of macrophages triggered by steatosis

in NAFLD, to the beneficial role in metabolic syndrome and type 2 diabetes played by M2 or alternatively activated macrophages (40). The reduced hepatocyte fat deposition upon GRK2 deletion may have helped suppress tissue inflammation by preventing either the recruitment or pro-inflammatory activation of macrophages (or both processes). Nevertheless, decreasing GRK2 abundance in macrophages themselves may also have a direct effect on the polarization or migration of these cells, a possibility that we are currently studying.

Overall, we suggest that GRK2, by directly inhibiting the insulin receptor cascade and controlling adrenergic receptor signaling, can regulate body weight gain, adiposity, metabolic rate and downstream targets of the insulin pathway in multiple tissues. Under pathological conditions, concurrent increases in GRK2 abundance in several tissues (9) would favor the development of an insulin-resistant phenotype, whereas decreasing GRK2 abundance could orchestrate a multi-organ anti-obesity response that collectively would reverse both systemic and tissue-specific features of such insulin-resistant and obese phenotype (Figure 6). Although we investigated here the impact of GRK2 deletion in WAT, BAT and liver, we cannot rule out additional effects of global GRK2 loss in other organs that could influence the observed phenotype, such as gut hormone production or sensitivity, sodium excretion, insulin synthesis, central effects, catecholamine concentrations and others.

At the molecular level, enhanced GRK2 abundance impairs insulin-mediated AKT stimulation and glucose uptake by interacting with IRS1 in adipocytes and myocytes (9), by directly phosphorylating IRS1 at Ser^{307} in cardiomyocytes (41), or by mediating insulin resistance induced by endothelin-1 by inhibiting both Gαq/11 and IRS1 pathways in 3T3-L1 adipocytes (42). Because HFD increases GRK2 abundance in WAT, muscle and liver (9), this inhibition of insulin signaling by GRK2 would be precluded in these key tissues with an efficient decrease in the amount of this kinase such as that observed in Tam-$GRK2^{-/-}$ mice.

Additional effects observed upon GRK2 deletion could be ascribed to increased adrenergic signaling related to the canonical function of GRK2 in βAR phosphorylation and desensitization. βARs are the main activators of the lipolytic process in WAT (43). Transgenic mice overexpressing β_1ARs have decreased adipose stores as a result of increased lipolytic activity and are resistant to becoming obese (44). Hence, the increased lipolysis in the WAT of Tam-$GRK2^{-/-}$ mice would be consistent with enhanced activation of adrenergic cascades upon GRK2 deletion, which would help correct the defective lipid mobilization and metabolism characteristic of obesity (45). However, a decompensated stimulation of the adrenergic axis can also have detrimental effects, because a long-term increase in circulating plasma concentrations of free fatty acids can indirectly stimulate *de novo* glucose synthesis, and β_2AR activation induces glycogenolysis and gluconeogenesis which may further exacerbate hepatic and skeletal muscle-based insulin resistance. Moreover, persistent sympathoadrenal activation is linked to glucose dysregulation and insulin resistance (46). Because insulin resistance did not occur upon GRK2 deletion, other compensatory mechanisms and tissue-specific effects must also be taking place.

One such compensatory mechanism could be increased BAT function. Sympathetic stimulation is critical for key effects of BAT on energy homeostasis including

thermogenesis (47) and glucose utilization (48). Moreover, activation and/or increased abundance of UCP1 may ameliorate impaired glucose metabolism caused by insulin resistance (49). Furthermore, whereas sympathetic over-activity might be associated with obesity (50), catecholamine sensitivity is decreased in the BAT of obese organisms (51). Therefore, enhanced adrenergic signaling in BAT upon decreasing GRK2 abundance, leading to increased CPT1 and UCP1, would not only promote enhanced fatty acid oxidation (which would help to prevent lipotoxicity caused by increased release of free fatty acids by WAT; Figure 6), but also contribute to the improved glucose homeostasis in Tam-GRK2$^{-/-}$ mice. Our data suggest that UCP1 abundance was increased by a post-transcriptional mechanism in the BAT of Tam-GRK2$^{-/-}$ mice. Because enhanced adrenergic activation, insulin and fatty acids inhibit proteolysis in BAT (52, 53), either enhanced insulin sensitivity or increased lipolytic capacity could be responsible for a reduced turnover rate of UCP1 in these mice. Because the main receptor subtype that mediates catecholamine-stimulated thermogenesis (24) and glucose uptake (54) in brown adipocytes is the β_3AR, which is resistant to agonist-induced desensitization and/or down-regulation (55), altered GRK2 abundance may impact BAT adrenergic pathways through alternative mechanisms downstream and/or independent from β_3AR that deserve further investigation.

Our present findings suggest that GRK2 may be a potential target for therapeutic intervention for metabolic syndrome. GRK2 has also been implicated in the modulation of insulin response in cardiac dysfunction (56) and hypertension (57, 58). Our experimental approach in decreasing GRK2 abundance in several tissues would mimic some aspects of the use of selective and effective GRK2 inhibitor, although the absence of the protein cannot fully recapitulate pharmacological inhibition. Accordingly, GRK2 peptide inhibitors improve parameters related to glucose homeostasis in animal models of diabetes (6), and exercise, which has a beneficial role in type 2 diabetes, reduces GRK2 abundance (59). It is tempting to suggest that selective peptide or small molecule inhibitors of GRK2 such as those being developed based on the crystal structures of this kinase (14, 60) could be used in the near future to further characterize the proof of concept results obtained in genetically-modified animal models, and that GRK2 inhibitors may hold great promise for the treatment of type 2 diabetes.

MATERIALS AND METHODS

Tam-GRK2$^{-/-}$ Mice

Floxed homozygous GRK2 mice (GRK2$^{fl/fl}$) (61) and transgenic mice overexpressing a Cre recombinase fused to a mutant form of the estrogen receptor (ER) to allow for tamoxifen-dependent activation [B6.Cg-Tg(CAGCre/Esr1* 5Amc/J] (62), were obtained from the Jackson Laboratories. Cre$^{+/-}$GRK2$^{fl/-}$ offsprings were backcrossed with GRK2$^{fl/fl}$ mice to obtain mice carrying both floxed GRK2 alleles and either none (Cre$^{-/-}$GRK2$^{fl/fl}$) or a single CreER allele (Cre$^{+/-}$GRK2$^{fl/fl}$). Recombination was induced by an intraperitoneal injection of tamoxifen (Tam) (Sigma-Aldrich, 2 mg/mouse, in saline containing 9% ethanol and 51% sunflower oil) for 5 consecutive days. Animals were genotyped by PCR on genomic DNA using reported oligonucleotides (61).

Animal Protocols

Mice were housed on a 12-hour light/dark cycle with free access to food and water in the animal facility of the University of Utrecht (the Netherlands). At 8 weeks of age, mice continued on a standard diet (SD) (2018S Harlan-Teklad, 12% calories from fat) or were fed a HFD (Sniff E15126-34, 52% calories from fat) during 8 weeks. At this time point, glucose tolerance tests (GTTs) and insulin tolerance tests (ITTs) were performed. HFD-fed mice were then injected with tamoxifen (Tam) and maintained on the HFD for 5 more weeks. Body weight and food intake were measured weekly. At the end of the HFD, GTT and ITT were repeated. For β-adrenergic blockade, mice were injected with propranolol (Sigma-Aldrich, 5mg/Kg body weight) one hour prior performing the GTT. Before sacrifice, mice were intraperitoneally injected with either vehicle (NaCl 0.9%) or insulin (Actrapid®, Novo Nordisk, 1 IU/Kg body weight). After 10 minutes, mice were euthanized, tissues were surgically removed, immediately weighted and either fixed or frozen in liquid nitrogen to be stored at −80°C. All experiments were performed in accordance with international guidelines and approved by the University Medical Center Utrecht and UAM experimental animal committee.

Metabolic assays

GTTs and ITTs were performed as previously described (9). Glucose (2g/Kg body weight) and insulin (0.8 U/kg body weight) were administered intraperitoneally. Glucose concentration was determined in tail blood samples using an automatic analyzer (One Touch Ultra), from Life Scan.

Plasma insulin concentration was measured by ELISA (Mercodia), and released non-esterified fatty acids (NEFA) was measured with an enzymatic method (NEFA-HR kit Wako Chemicals).

Adipocyte Size Determination

Adipose tissue sections were stained with haematoxylin and eosin for the evaluation of adipocyte size. Individual adipocyte areas within each field were determined using image analysis software (ImageJ). Relative adipocyte size was calculated in arbitrary fields by quantitation of 150 cells in at least four different randomly chosen fields per mouse.

Ex vivo lipolysis

Epididymal white and brown fat pads were isolated from 12h-fasted mice and sliced into equal-sized pieces of ~50 mg and ~20 mg respectively. Explants were washed twice in PBS and stimulated with isoproterenol (10 μM, Sigma-Aldrich) for 2h at 37°C in 0.5 ml of DMEM supplemented with 1% FA-free BSA. NEFA release was measured following manufacturer's indications (NEFA-HR kit Wako Chemicals) in aliquots from incubation media at 0 and 120 min, and was normalized relative to tissue weight.

Immunohistochemical detection of the F4/80 macrophage marker and quantification of hepatic “crown-like structures” (hCLS)

Liver tissue sections were de-paraffinized and rehydrated, and slides were incubated overnight with the primary antibody anti-F4/80 (clone BM8, Abcam) to perform immunohistochemical detection as previously described (63, 64). The absence of the primary antibody was used as negative control. The presence of macrophages (F4/80 staining positive area) was determined using image analysis software (ImageJ). Three to five different high-power fields from each section were analyzed per animal. The number of hCLS in the whole area of each F4/80-stained section was quantified and expressed as the mean number/mm^2.

Western Blot analysis

Tissues were homogenized using metal beads in a Tissue Lyser as previously described (65). 30–50 μg of total protein was resolved per lane by SDS-PAGE and transferred to a nitrocellulose membrane. Blots were probed with specific antibodies against phosphorylated (Ser^{473}) and total AKT, phosphorylated (Thr^{183}/Tyr^{185}) and total JNK1/2 (Cell Signalling), C/EBPα, PPARγ, GRK2 (Santa Cruz), HSL and GAPDH (Abcam) as previously described (63). Equal amounts of protein as determined by the DC protein assay method (Bio-Rad) were loaded per lane. Equivalent loading was further assessed by Ponceau staining and GAPDH abundance. Immunoreactive bands were visualized using enhanced chemiluminescence (ECL; Amersham Biosciences) or the Odissey Infrared Imaging System (Li-Cor Biosciences). Films were scanned with a GS-700 Imaging Densitometer and analyzed with Quantity One Software (Bio-Rad), or using an Odissey Classic reader and the Odissey software package 3.0 (Li-Cor Biosciences).

mRNA isolation and Real Time PCR

RNA was extracted using metal beads in a Tissue Lyser and the RNeasy Mini Kit (Qiagen) following the instructions provided by the supplier. Quantity and quality of RNA were analyzed using Nanodrop ND-1000 (Thermo Scientific).

RT-PCRs were performed in the Genomic Facility at CBMSO using Light Cycler equipment (Roche) and primers labeled with Syber Green (Supplementary Table 1) (Sigma).

A geometric mean of three stably expressed and commonly used reference genes (*ywhaz*, *gapdh* and *18s*) was used for data normalization in the liver and a geometric mean of two (*ppia* and *b2m*) was used for data normalization in WAT and BAT. qPCRs and statistical analysis of the data were performed using GenEx software.

Data analysis

All data are expressed as mean values ± SEM and n represents the number of animals. Normal distribution was determined using a Shapiro-Wilk normality test prior to statistical analysis. Whenever normality test was positive, statistical significance was analyzed by using unpaired Student’s t test or one- or two-way repeated measures ANOVA followed by Bonferroni’s *post hoc* test. When the normality test was not positive, or when significant differences were found between variances (determined by Bartletts’ or by F-test of equality

of variances), statistical significance was analyzed using Mann-Whitney test, unpaired t test with Welch's correction or Kruskal Wallis followed by Dunn's Multiple Comparison Test. Differences were considered statistically significant when P value <0.05.

Supplementary Material

Refer to Web version on PubMed Central for supplementary material.

Acknowledgments

We greatly appreciate the help and advice regarding statistical analysis of this work from Lorena Piris, from the Methodology Support Unit of the IIS La Princesa, Madrid. We thank Dr. Huijing Wang and Sabine Versteeg, University Medical Center Utrecht, The Netherlands for their technical and experimental help. Also, we thank the genomic facility at the Centro de Biología Molecular Severo Ochoa.

Funding: This work was supported by Grants SAF2014-55511-R (to F.M and C. M.) from Ministerio de Economía y Competitividad (MINECO), Spain; S2010/BMD-2332 (INDISNET) from Comunidad de Madrid, Spain (to FM); The Cardiovascular Network (RD12/0042/0012), from Ministerio Sanidad y Consumo-Instituto Carlos III, Spain (to FM), an European Foundation for the Study of Diabetes (EFSD) Novo Nordisk Partnership for Diabetes Research in Europe Grant (to FM); Fundación Ramón Areces (to C. M.); the National Institute of Neurological Disorders and Stroke of the National Institutes of Health under award numbers RO1NS073939 and RO1NS074999; and by a STAR award of the University of Texas Systems. ELF was recipient of a FPU fellowship from Ministerio de Educación-Spain; MCS is recipient of a FPI fellowship from Universidad Autónoma Madrid. We also acknowledge the support of a Contrato para la Formación Postdoctoral from MINECO and of an EMBO short-term fellowship to RVB, and institutional support from Fundación Ramón Areces.

REFERENCES AND NOTES

1. Eckardt K, Taube A, Eckel J. Obesity-associated insulin resistance in skeletal muscle: role of lipid accumulation and physical inactivity. Rev Endocr Metab Disord. 2011; 12:163–172. [PubMed: 21336841]
2. Ribas C, Penela P, Murga C, Salcedo A, Garcia-Hoz C, Jurado-Pueyo M, Aymerich I, Mayor F Jr. The G protein-coupled receptor kinase (GRK) interactome: role of GRKs in GPCR regulation and signaling. Biochim Biophys Acta. 2007; 1768:913–922. [PubMed: 17084806]
3. Penela P, Murga C, Ribas C, Lafarga V, Mayor F Jr. The complex G protein-coupled receptor kinase 2 (GRK2) interactome unveils new physiopathological targets. Br J Pharmacol. 2010; 160:821–832. [PubMed: 20590581]
4. Gurevich EV, Tesmer JJ, Mushegian A, Gurevich VV. G protein-coupled receptor kinases: more than just kinases and not only for GPCRs. Pharmacol Ther. 2012; 133:40–69. [PubMed: 21903131]
5. Evron T, Daigle TL, Caron MG. GRK2: multiple roles beyond G protein-coupled receptor desensitization. Trends Pharmacol Sci. 2012; 33:154–164. [PubMed: 22277298]
6. Anis Y, Leshem O, Reuveni H, Wexler I, Ben Sasson R, Yahalom B, Laster M, Raz I, Ben Sasson S, Shafrir E, Ziv E. Antidiabetic effect of novel modulating peptides of G-protein-coupled kinase in experimental models of diabetes. Diabetologia. 2004; 47:1232–1244. [PubMed: 15235770]
7. Mayor F Jr, Lucas E, Jurado-Pueyo M, Garcia-Guerra L, Nieto-Vazquez I, Vila-Bedmar R, Fernandez-Veledo S, Murga C. G Protein-coupled receptor kinase 2 (GRK2): A novel modulator of insulin resistance. Arch Physiol Biochem. 2011; 117:125–130. [PubMed: 21615207]
8. Ciccarelli M, Cipolletta E, Iaccarino G. GRK2 at the control shaft of cellular metabolism. Curr Pharm Des. 2012; 18:121–127. [PubMed: 22229580]
9. Garcia-Guerra L, Nieto-Vazquez I, Vila-Bedmar R, Jurado-Pueyo M, Zalba G, Diez J, Murga C, Fernandez-Veledo S, Mayor F Jr, Lorenzo M. G protein-coupled receptor kinase 2 plays a relevant role in insulin resistance and obesity. Diabetes. 2010; 59:2407–2417. [PubMed: 20627936]
10. Vila-Bedmar R, Garcia-Guerra L, Nieto-Vazquez I, Mayor F Jr, Lorenzo M, Murga C, Fernandez-Veledo S. GRK2 contribution to the regulation of energy expenditure and brown fat function. FASEB J. 2012; 26:3503–3514. [PubMed: 22516294]

11. Cipolletta E, Campanile A, Santulli G, Sanzari E, Leosco D, Campiglia P, Trimarco B, Iaccarino G. The G protein coupled receptor kinase 2 plays an essential role in beta-adrenergic receptor-induced insulin resistance. Cardiovasc Res. 2009; 84:407–415. [PubMed: 19620130]
12. Fu Q, Xu B, Liu Y, Parikh D, Li J, Li Y, Zhang Y, Riehle C, Zhu Y, Rawlings T, Shi Q, Clark RB, Chen X, Abel ED, Xiang YK. Insulin inhibits cardiac contractility by inducing a Gi-biased beta2 adrenergic signaling in hearts. Diabetes. 2014
13. Carotenuto A, Cipolletta E, Gomez-Monterrey I, Sala M, Vernieri E, Limatola A, Bertamino A, Musella S, Sorriento D, Grieco P, Trimarco B, Novellino E, Iaccarino G, Campiglia P. Design, synthesis and efficacy of novel G protein-coupled receptor kinase 2 inhibitors. Eur J Med Chem. 2013; 69:384–392. [PubMed: 24077529]
14. Homan KT, Tesmer JJ. Molecular Basis for Small Molecule Inhibition of G Protein-Coupled Receptor Kinases. ACS Chem Biol. 2014
15. Lee KY, Russell SJ, Ussar S, Boucher J, Vernochet C, Mori MA, Smyth G, Rourk M, Cederquist C, Rosen ED, Kahn BB, Kahn CR. Lessons on conditional gene targeting in mouse adipose tissue. Diabetes. 2013; 62:864–874. [PubMed: 23321074]
16. Wang H, Heijnen CJ, Eijkelkamp N, Garza Carbajal A, Schedlowski M, Kelley KW, Dantzer R, Kavelaars A. GRK2 in sensory neurons regulates epinephrine-induced signalling and duration of mechanical hyperalgesia. Pain. 2011; 152:1649–1658. [PubMed: 21514055]
17. Owen C, Lees EK, Grant L, Zimmer DJ, Mody N, Bence KK, Delibegovic M. Inducible liver-specific knockdown of protein tyrosine phosphatase 1B improves glucose and lipid homeostasis in adult mice. Diabetologia. 2013; 56:2286–2296. [PubMed: 23832083]
18. DeFronzo RA, Tripathy D. Skeletal muscle insulin resistance is the primary defect in type 2 diabetes. Diabetes Care. 2009; 32(Suppl 2):S157–163. [PubMed: 19875544]
19. Rosen ED, MacDougald OA. Adipocyte differentiation from the inside out. Nat Rev Mol Cell Biol. 2006; 7:885–896. [PubMed: 17139329]
20. Granneman JG, Moore HP. Location, location: protein trafficking and lipolysis in adipocytes. Trends Endocrinol Metab. 2008; 19:3–9. [PubMed: 18155916]
21. Cypess AM, Kahn CR. Brown fat as a therapy for obesity and diabetes. Curr Opin Endocrinol Diabetes Obes. 2010; 17:143–149. [PubMed: 20160646]
22. Vila-Bedmar R, Fernandez-Veledo S. A new era for brown adipose tissue: New insights into brown adipocyte function and differentiation. Arch Physiol Biochem. 2011; 117:195–208. [PubMed: 21428723]
23. McGarry JD, Brown NF. The mitochondrial carnitine palmitoyltransferase system. From concept to molecular analysis. Eur J Biochem. 1997; 244:1–14. [PubMed: 9063439]
24. Cannon B, Nedergaard J. Brown adipose tissue: function and physiological significance. Physiol Rev. 2004; 84:277–359. [PubMed: 14715917]
25. Lowell BB, Spiegelman BM. Towards a molecular understanding of adaptive thermogenesis. Nature. 2000; 404:652–660. [PubMed: 10766252]
26. Obregon MJ. Adipose tissues and thyroid hormones. Front Physiol. 2014; 5:479. [PubMed: 25566082]
27. Richard D, Carpentier AC, Dore G, Ouellet V, Picard F. Determinants of brown adipocyte development and thermogenesis. Int J Obes (Lond). 2010; 34(Suppl 2):S59–66. [PubMed: 21151149]
28. Kohjima M, Enjoji M, Higuchi N, Kato M, Kotoh K, Yoshimoto T, Fujino T, Yada M, Yada R, Harada N, Takayanagi R, Nakamuta M. Re-evaluation of fatty acid metabolism-related gene expression in nonalcoholic fatty liver disease. Int J Mol Med. 2007; 20:351–358. [PubMed: 17671740]
29. Inoue M, Ohtake T, Motomura W, Takahashi N, Hosoki Y, Miyoshi S, Suzuki Y, Saito H, Kohgo Y, Okumura T. Increased expression of PPARgamma in high fat diet-induced liver steatosis in mice. Biochem Biophys Res Commun. 2005; 336:215–222. [PubMed: 16125673]
30. Smith BW, Adams LA. Nonalcoholic fatty liver disease and diabetes mellitus: pathogenesis and treatment. Nature reviews Endocrinology. 2011; 7:456–465.

31. Cinti S, Mitchell G, Barbatelli G, Murano I, Ceresi E, Faloia E, Wang S, Fortier M, Greenberg AS, Obin MS. Adipocyte death defines macrophage localization and function in adipose tissue of obese mice and humans. J Lipid Res. 2005; 46:2347–2355. [PubMed: 16150820]
32. Weston CR, Davis RJ. The JNK signal transduction pathway. Curr Opin Cell Biol. 2007; 19:142–149. [PubMed: 17303404]
33. Bergman RN, Ader M. Free fatty acids and pathogenesis of type. 2 diabetes mellitus. Trends Endocrinol Metab. 2000; 11:351–356. [PubMed: 11042464]
34. Samocha-Bonet D, Chisholm DJ, Tonks K, Campbell LV, Greenfield JR. Insulin-sensitive obesity in humans - a 'favorable fat' phenotype? Trends Endocrinol Metab. 2012; 23:116–124. [PubMed: 22284531]
35. Girousse A, Tavernier G, Valle C, Moro C, Mejhert N, Dinel AL, Houssier M, Roussel B, Besse-Patin A, Combes M, Mir L, Monbrun L, Bezaire V, Prunet-Marcassus B, Waget A, Vila I, Caspar-Bauguil S, Louche K, Marques MA, Mairal A, Renoud ML, Galitzky J, Holm C, Mouisel E, Thalamas C, Viguerie N, Sulpice T, Burcelin R, Arner P, Langin D. Partial inhibition of adipose tissue lipolysis improves glucose metabolism and insulin sensitivity without alteration of fat mass. PLoS Biol. 2013; 11:e1001485. [PubMed: 23431266]
36. Galgani JE, Moro C, Ravussin E. Metabolic flexibility and insulin resistance. Am J Physiol Endocrinol Metab. 2008; 295:E1009–1017. [PubMed: 18765680]
37. Vidal-Puig A, Jimenez-Linan M, Lowell BB, Hamann A, Hu E, Spiegelman B, Flier JS, Moller DE. Regulation of PPAR gamma gene expression by nutrition and obesity in rodents. J Clin Invest. 1996; 97:2553–2561. [PubMed: 8647948]
38. Gordon S. Alternative activation of macrophages. Nat Rev Immunol. 2003; 3:23–35. [PubMed: 12511873]
39. Itoh M, Kato H, Suganami T, Konuma K, Marumoto Y, Terai S, Sakugawa H, Kanai S, Hamaguchi M, Fukaishi T, Aoe S, Akiyoshi K, Komohara Y, Takeya M, Sakaida I, Ogawa Y. Hepatic crown-like structure: a unique histological feature in non-alcoholic steatohepatitis in mice and humans. PLoS One. 2013; 8:e82163. [PubMed: 24349208]
40. Odegaard JI, Ricardo-Gonzalez RR, Red Eagle A, Vats D, Morel CR, Goforth MH, Subramanian V, Mukundan L, Ferrante WA, Chawla A. Alternative M2 activation of Kupffer cells by PPARdelta ameliorates obesity-induced insulin resistance. Cell Metab. 2008; 7:496–507. [PubMed: 18522831]
41. Ciccarelli M, Chuprun JK, Rengo G, Gao E, Wei Z, Peroutka RJ, Gold JI, Gumpert A, Chen M, Otis NJ, Dorn GW 2nd, Trimarco B, Iaccarino G, Koch WJ. G protein-coupled receptor kinase 2 activity impairs cardiac glucose uptake and promotes insulin resistance after myocardial ischemia. Circulation. 2011; 123:1953–1962. [PubMed: 21518983]
42. Usui I, Imamura T, Babendure JL, Satoh H, Lu JC, Hupfeld CJ, Olefsky JM. G protein-coupled receptor kinase 2 mediates endothelin-1-induced insulin resistance via the inhibition of both Galphaq/11 and insulin receptor substrate-1 pathways in 3T3-L1 adipocytes. Mol Endocrinol. 2005; 19:2760–2768. [PubMed: 15994203]
43. Collins S. beta-Adrenoceptor Signaling Networks in Adipocytes for Recruiting Stored Fat and Energy Expenditure. Front Endocrinol (Lausanne). 2011; 2:102. [PubMed: 22654837]
44. Soloveva V, Graves RA, Rasenick MM, Spiegelman BM, Ross SR. Transgenic mice overexpressing the beta 1-adrenergic receptor in adipose tissue are resistant to obesity. Mol Endocrinol. 1997; 11:27–38. [PubMed: 8994185]
45. Gaidhu MP, Anthony NM, Patel P, Hawke TJ, Ceddia RB. Dysregulation of lipolysis and lipid metabolism in visceral and subcutaneous adipocytes by high-fat diet: role of ATGL, HSL, and AMPK. Am J Physiol Cell Physiol. 2010; 298:C961–971. [PubMed: 20107043]
46. Boyda HN, Procyshyn RM, Pang CC, Barr AM. Peripheral adrenoceptors: the impetus behind glucose dysregulation and insulin resistance. J Neuroendocrinol. 2013; 25:217–228. [PubMed: 23140239]
47. Collins S, Yehuda-Shnaidman E, Wang H. Positive and negative control of Ucp1 gene transcription and the role of beta-adrenergic signaling networks. Int J Obes (Lond). 2010; 34(Suppl 1):S28–33. [PubMed: 20935662]

48. Orava J, Nuutila P, Lidell ME, Oikonen V, Noponen T, Viljanen T, Scheinin M, Taittonen M, Niemi T, Enerback S, Virtanen KA. Different metabolic responses of human brown adipose tissue to activation by cold and insulin. Cell Metab. 2011; 14:272–279. [PubMed: 21803297]

49. Inokuma K, Ogura-Okamatsu Y, Toda C, Kimura K, Yamashita H, Saito M. Uncoupling protein 1 is necessary for norepinephrine-induced glucose utilization in brown adipose tissue. Diabetes. 2005; 54:1385–1391. [PubMed: 15855324]

50. Lambert GW, Straznicky NE, Lambert EA, Dixon JB, Schlaich MP. Sympathetic nervous activation in obesity and the metabolic syndrome--causes, consequences and therapeutic implications. Pharmacol Ther. 2010; 126:159–172. [PubMed: 20171982]

51. Marette A, Geloen A, Collet A, Bukowiecki LJ. Defective metabolic effects of norepinephrine and insulin in obese Zucker rat brown adipose tissue. Am J Physiol. 1990; 258:E320–328. [PubMed: 2154935]

52. Moazed B, Desautels M. Control of proteolysis by norepinephrine and insulin in brown adipocytes: role of ATP, phosphatidylinositol 3-kinase, and p70 S6K. Can J Physiol Pharmacol. 2002; 80:541–552. [PubMed: 12117303]

53. Azzu V, Jastroch M, Divakaruni AS, Brand MD. The regulation and turnover of mitochondrial uncoupling proteins. Biochim Biophys Acta. 2010; 1797:785–791. [PubMed: 20211596]

54. Dallner OS, Chernogubova E, Brolinson KA, Bengtsson T. Beta3-adrenergic receptors stimulate glucose uptake in brown adipocytes by two mechanisms independently of glucose transporter 4 translocation. Endocrinology. 2006; 147:5730–5739. [PubMed: 16959848]

55. Liggett SB, Freedman NJ, Schwinn DA, Lefkowitz RJ. Structural basis for receptor subtype-specific regulation revealed by a chimeric beta 3/beta 2-adrenergic receptor. Proc Natl Acad Sci USA. 1993; 90:3665–3669. [PubMed: 8386380]

56. Lymperopoulos A, Rengo G, Koch WJ. GRK2 inhibition in heart failure: something old, something new. Curr Pharm Des. 2012; 18:186–191. [PubMed: 22229578]

57. Taguchi K, Matsumoto T, Kamata K, Kobayashi T. G protein-coupled receptor kinase 2, with beta-arrestin 2, impairs insulin-induced Akt/endothelial nitric oxide synthase signaling in ob/ob mouse aorta. Diabetes. 2012; 61:1978–1985. [PubMed: 22688330]

58. Avendano MS, Lucas E, Jurado-Pueyo M, Martinez-Revelles S, Vila-Bedmar R, Mayor F Jr, Salaices M, Briones AM, Murga C. Increased nitric oxide bioavailability in adult GRK2 hemizygous mice protects against angiotensin II-induced hypertension. Hypertension. 2014; 63:369–375. [PubMed: 24191280]

59. Leosco D, Rengo G, Iaccarino G, Filippelli A, Lymperopoulos A, Zincarelli C, Fortunato F, Golino L, Marchese M, Esposito G, Rapacciuolo A, Rinaldi B, Ferrara N, Koch WJ, Rengo F. Exercise training and beta-blocker treatment ameliorate age-dependent impairment of beta-adrenergic receptor signaling and enhance cardiac responsiveness to adrenergic stimulation. Am J Physiol Heart Circ Physiol. 2007; 293:H1596–1603. [PubMed: 17557919]

60. Schumacher SM, Gao E, Zhu W, Chen X, Chuprun JK, Feldman AM, GTJJ, Koch WJ. Paroxetine-mediated GRK2 inhibition reverses cardiac dysfunction and remodeling after myocardial infarction. Sci Transl Med. 2015; 7:277ra231.

61. Rivas V, Carmona R, Munoz-Chapuli R, Mendiola M, Nogues L, Reglero C, Miguel-Martin M, Garcia-Escudero R, Dorn GW 2nd, Hardisson D, Mayor F Jr, Penela P. Developmental and tumoral vascularization is regulated by G protein-coupled receptor kinase 2. J Clin Invest. 2013; 123:4714–4730. [PubMed: 24135140]

62. Hayashi S, McMahon AP. Efficient recombination in diverse tissues by a tamoxifen-inducible form of Cre: a tool for temporally regulated gene activation/inactivation in the mouse. Dev Biol. 2002; 244:305–318. [PubMed: 11944939]

63. Vila-Bedmar R, Lorenzo M, Fernandez-Veledo S. Adenosine 5′-monophosphate-activated protein kinase-mammalian target of rapamycin cross talk regulates brown adipocyte differentiation. Endocrinology. 2010; 151:980–992. [PubMed: 20133456]

64. Garcia-Guerra L, Vila-Bedmar R, Carrasco-Rando M, Cruces-Sande M, Martin M, Ruiz-Gomez A, Ruiz-Gomez M, Lorenzo M, Fernandez-Veledo S, Mayor F Jr, Murga C, Nieto-Vazquez I. Skeletal muscle myogenesis is regulated by G protein-coupled receptor kinase 2. J Mol Cell Biol. 2014; 6:299–311. [PubMed: 24927997]

65. Lucas E, Jurado-Pueyo M, Fortuno MA, Fernandez-Veledo S, Vila-Bedmar R, Jimenez-Borreguero LJ, Lazcano JJ, Gao E, Gomez-Ambrosi J, Fruhbeck G, Koch WJ, Diez J, Mayor F Jr, Murga C. Downregulation of G protein-coupled receptor kinase 2 levels enhances cardiac insulin sensitivity and switches on cardioprotective gene expression patterns. Biochim Biophys Acta. 2014; 1842:2448–2456. [PubMed: 25239306]

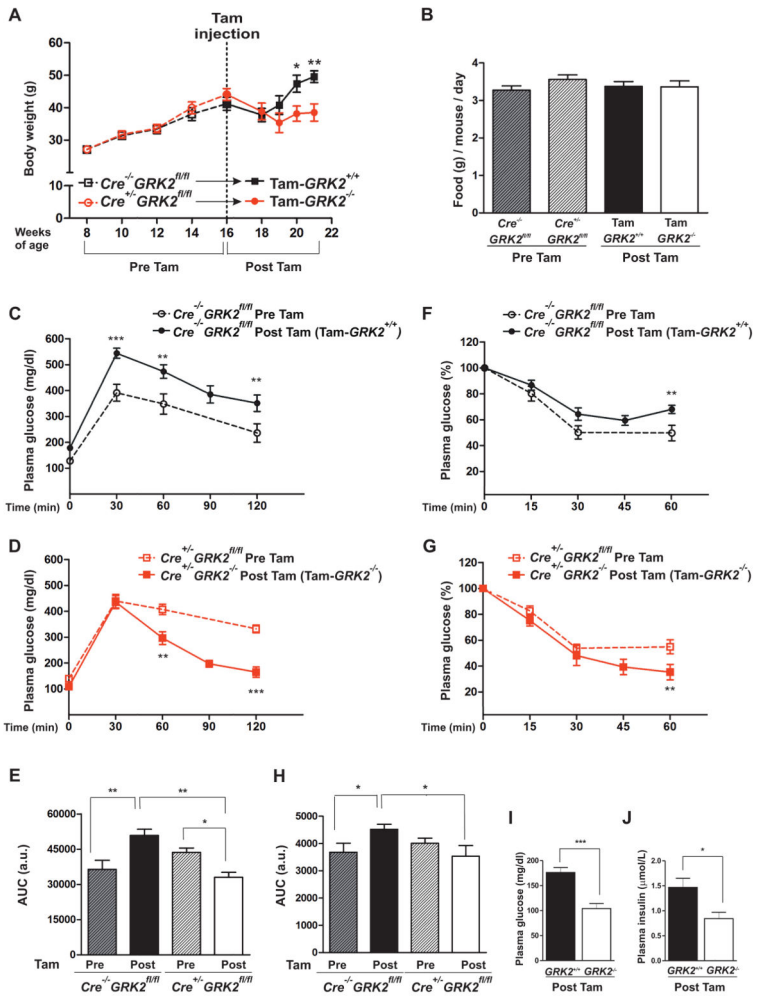

Figure 1. Tamoxifen-induced GRK2 ablation prevents diet-induced obesity and reverses HFD-induced glucose intolerance

Mice were fed a HFD for 8 weeks, injected with tamoxifen and maintained for 5 more weeks on the HFD. (**A**) Body weight evolution (expressed in g) along the 13 weeks of high fat feeding. (**B**) Daily food intake: no significant differences were found between any pair of conditions. **(C and D)** Intraperitoneal glucose tolerance tests (GTTs) were performed either at 8 weeks of HFD (before tamoxifen administration, dotted lines) or 5 weeks after tamoxifen injection, following a total of 13 weeks of HFD (solid lines) in control ($Cre^{-/-}GRK2^{fl/fl}$) mice (C, black), and $Cre^{+/-}GRK2^{fl/fl}$ mice (D panel, red). (**E**) Histogram showing the GTT area under the curve (AUC) of data in (C) and (D). **(F and G)** Insulin tolerance tests (ITTs) were performed in mice described in (C) and (D), before and after tamoxifen treatment. **(H)** Histogram showing the ITT area under the curve of data in (F) and (G). **(I and J)** Serum concentrations of fasting glucose (**I**) and insulin (**J**) from HFD-fed control ($Cre^{-/-}GRK2^{fl/fl}$) and Tam-$GRK2^{-/-}$ mice. Results in (A) to (J) are means ± SEM of 7–8 mice per group. Statistical analysis was performed by two-way repeated measures ANOVA followed by Bonferroni's *post hoc* test (A–H) or by unpaired two-tailed t test (I–J).

*P < 0.05; **P < 0.01. Open symbols, dotted lines = Pre-Tam; filled symbols, solid lines = Post-Tam; Black = $Cre^{-/-}GRK2^{fl/fl}$; Red = $Cre^{+/-}GRK2^{fl/fl}$)

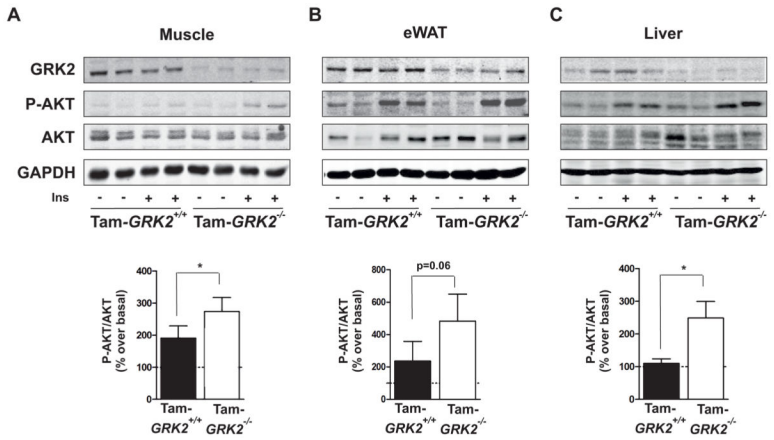

Figure 2. GRK2 loss during a HFD enhances insulin signalling in insulin-sensitive tissues

(A) to (C) Following the 13 weeks of HFD control and Tam-GRK2$^{-/-}$ mice were treated with either vehicle or insulin and tissue lysates from muscle (**A**), eWAT (**B**) and liver (**C**) were subjected to Western blot and probed with antibodies against GRK2, total and phosphorylated AKT (Ser^{473}), and GAPDH. Representative immunoblots and densitometric analysis of four mice per group are shown. Results are expressed as % of stimulation over vehicle-treated mice (basal). Results are means ± SEM of 7–8 mice per genotype, 3–4 mice per treatment. Statistical significance was analyzed by unpaired two-tailed t test (A) and (C) or by Mann-Whitney test (B). *P < 0.05.

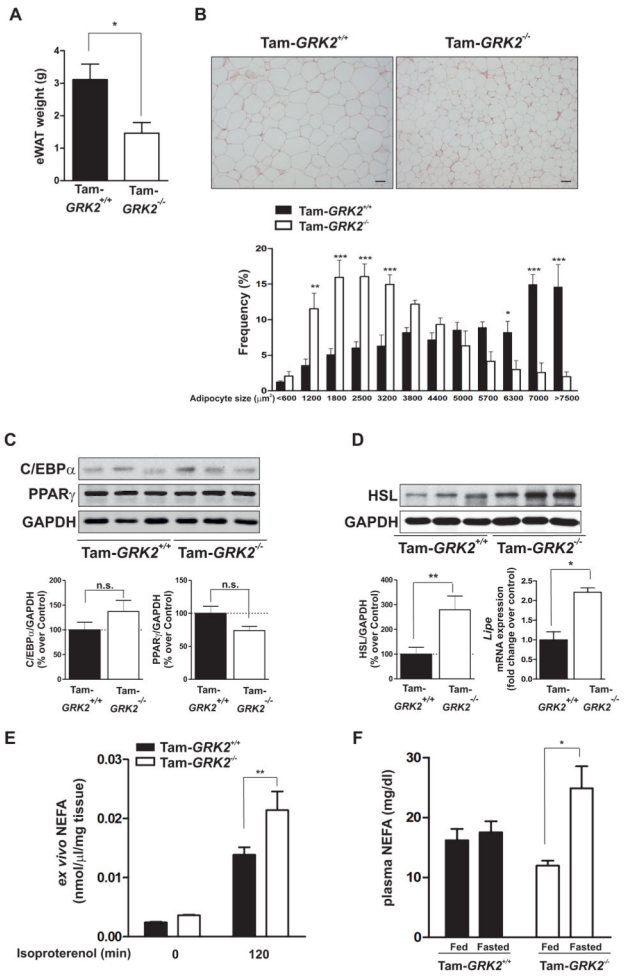

Figure 3. Tamoxifen-induced GRK2 depletion reduces epididymal adipose mass and adipocyte size and increases markers of lipolysis

(**A**) eWAT weight in control (Tam-GRK2$^{+/+}$) and Tam-GRK2$^{-/-}$ mice at the end of the 13-week HFD. (**B**) Sections of epididymal fat pads from control and Tam-GRK2$^{-/-}$ mice stained with hematoxylin and eosin (magnification ×10; scale bar 50 μm). Representative photomicrographs are shown. Relative adipocyte size was calculated by determining individual adipocyte areas using image analysis software (ImageJ) in at least four different randomly chosen fields per mouse, in 5 mice per genotype. (**C**) eWAT lysates were immunoblotted for PPARγ, C/EBPα, and FAS using GAPDH as a loading control. Representative immunoblots and densitometric analysis are shown. D) eWAT lysates were immunoblotted for HSL and subjected to real-time quantitative polymerase chain reaction (qPCR) to measure the expression of HSL (*lipe*). qPCR results were normalized against *ppia* and *b2m* mRNAs. Data are represented as means ± SEM of 7–8 mice per genotype for (B) and (C) and 6 mice per genotype for (D). Statistical significance was analyzed by unpaired two-tailed t test. *P < 0.05; **P < 0.01; ***P<0.005. **(E)** Non-esterified fatty acid (NEFA) release from eWAT explants isolated from control or Tam-GRK2$^{-/-}$ mice (N=4–6 per genotype) was measured in supernatants at the indicated times of isoproterenol stimulation. (**F**) Circulating non-esterified fatty acid serum concentrations in 13-week HFD-fed controls

and Tam-GRK2$^{-/-}$ mice either fed or fasted for 16 hours. Data are represented as means ± SEM of 4–5 mice per group. Statistical significance was analyzed by 2-way ANOVA followed by Bonferroni *post-hoc* test (E) and by Kruskal Wallis followed by Dunn's Multiple Comparison Test (F) **P < 0.01.*P < 0.05; **P < 0.01.

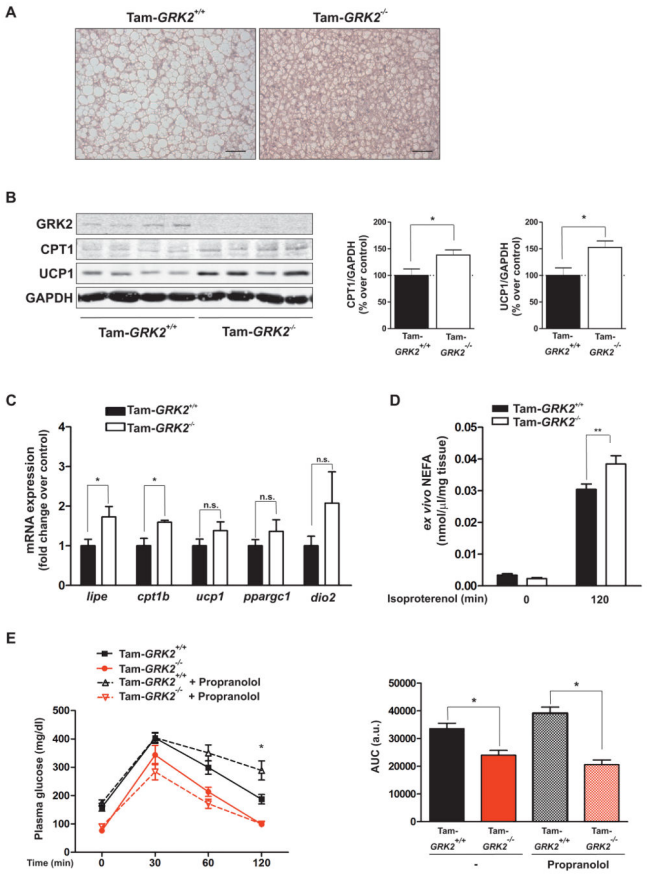

Figure 4. Decreasing GRK2 abundance during a HFD prevents fat accumulation within BAT and augments the expression of fatty acid oxidation and thermogenic markers

(**A**) Sections of BAT from control (Tam-GRK2$^{+/+}$) and Tam-GRK2$^{-/-}$ mice after 13 weeks of HFD were stained with hematoxylin and eosin (scale bar 50 μm). Representative photomicrographs from 5 mice per genotype are shown. (**B**) BAT lysates were immunoblotted for GRK2, CPT1, UCP1 and GAPDH. Representative immunoblots and densitometric analysis are shown. (**C**) qPCR was used to measure the expression of HSL (*lipe*), CPT1 (*cpt1b*), UCP1 (*ucp1*), PGC1α (*ppargc1a*) and Dio2 (*dio2*) mRNAs. Results were normalized against *ppia* and *b2m* mRNAs. Data are means ± SEM of 7–8 mice per genotype for (B) and 6 mice per genotype for (C). Statistical significance was analyzed by unpaired two tailed t test. *P < 0.05. **(D)** NEFA release from interscapular BAT explants isolated from control or Tam-GRK2$^{-/-}$ mice (N=4–6 mice per genotype) was measured in supernatants at the indicated times after isoproterenol stimulation. Statistical significance was analyzed by 2-way ANOVA followed by Bonferroni *post-hoc* test **P < 0.01. **(E)** Intraperitoneal glucose tolerance tests (GTTs) were performed in mice treated or not with propranolol before the GTTs. Histogram shows the GTT area under the curve (AUC). Results are means ± SEM of 4–6 mice per group. Statistical analysis was performed by two-way repeated measures ANOVA followed by Bonferroni's *post hoc* test. *P < 0.05. Open symbols, dotted lines = Propranolol-treated; filled symbols, solid lines = No treatment; Black = Tam-GRK2$^{+/+}$; Red = Tam-GRK2$^{-/-}$)

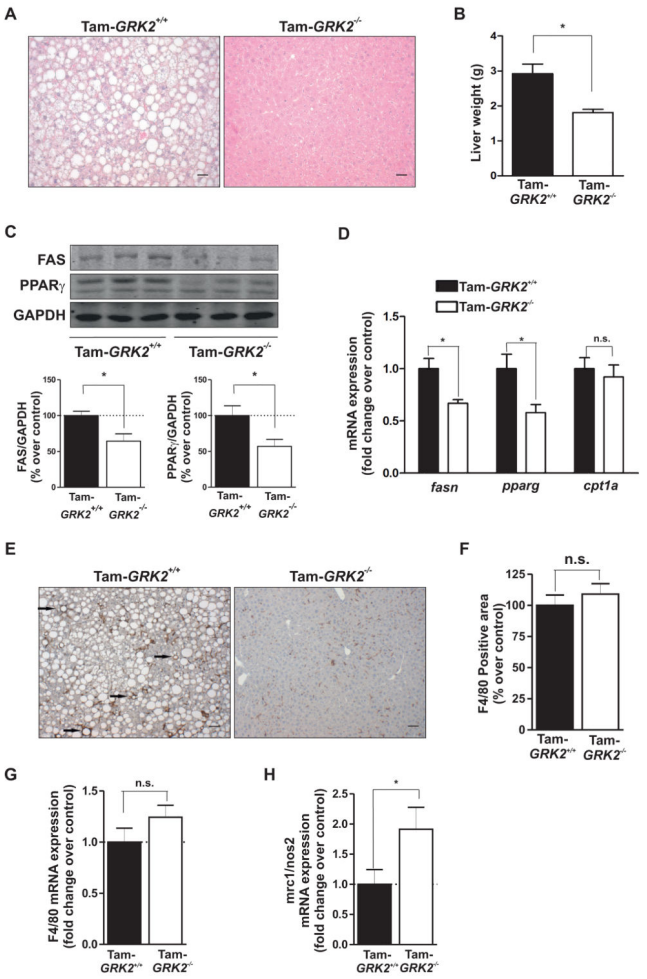

Figure 5. Tamoxifen-induced GRK2 loss protects against the development of NAFLD and associated inflammation in the liver

(**A**) Liver sections from HFD-fed control ($Cre^{-/-}GRK2^{fl/fl}$) and Tam-$GRK2^{-/-}$ mice were stained with hematoxylin and eosin (scale bar 50 μm). Images are representative of 4–5 mice per genotype. (**B**) Liver weight in control and Tam-$GRK2^{-/-}$ mice. (**C**) Representative immunoblots and densitometric analysis are shown for FAS, PPARγ and GAPDH. (**D**) qPCR was used to measure the expression of mRNAs encoding PPARγ (*pparg*), FAS (*fasn*) and CPT1 (*cpt1a*). Results were normalized against *ywhaz* and *gapdh* mRNAs. Data in (B), (C), and (E) are means ± SEM of 7–8 mice per genotype. (**E and F**) Immunohistochemical analysis of liver sections stained with F4/80 antibody and counterstained with hematoxylin. Representative photomicrographs are shown and characteristic macrophage arrangements known as hepatic crown-like structures (hCLS) are indicated by arrows (E). Positively stained area was quantified using Image J Software in at least four different randomly chosen fields per mouse, in 4–5 mice per genotype (F). (**G** and **H**) qPCR was used to measure the hepatic expression of the F4/80-encoding mRNA (G) and the ratio between mRNAs encoding mannose receptor C type 1 (*mrc1*), and inducible nitric oxide synthase (*nos2*) as M2 and M1 markers respectively (H). Results were normalized against *ywhaz* and *gapdh* mRNAs. Values are represented as fold change over control mice and are means ±

SEM of 6 mice per genotype. Statistical significance was analyzed by unpaired two-tailed t test. *P <0.05.

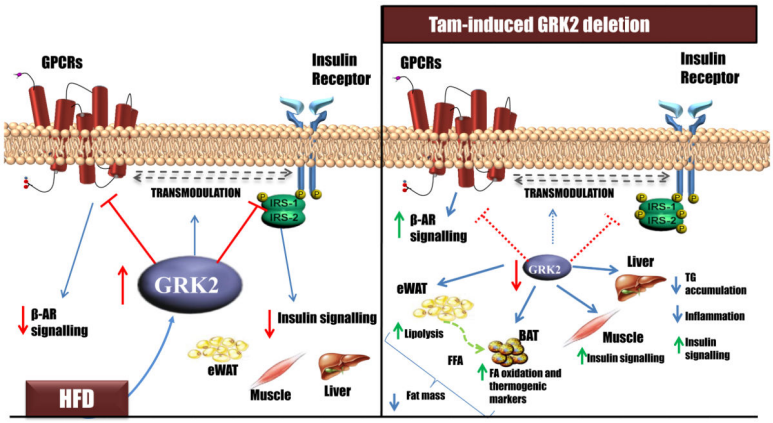

Figure 6. GRK2 depletion during the course of a HFD can reverse an already established obese and insulin resistant phenotype, potentially through its combined effects in different tissues

Besides its role as a GPCR kinase, GRK2 inhibits insulin signalling and may also control the GPCR-mediated transmodulation of the insulin pathway. A reduction in GRK2 abundance after obesity and insulin resistance have been established leads to: (i) an increased adrenergic-dependent lipolytic capacity in eWAT that provides BAT with free fatty acids. In turn, BAT displays an enhanced expression of oxidative and thermogenic markers, and consequently both tissues may contribute to the concerted protection against excessive fat mass accretion; (ii) improved insulin signalling in muscle which can underlie the enhanced insulin-induced glucose clearance; (iii) increased insulin signalling in liver associated with a decrease in triacylglyceride accumulation and inflammation within this tissue. All these processes may mediate the protective effects of lowering GRK2 abundance against excessive body weight gain and HFD-induced insulin resistance.